



OPEN

# Frustrated hierarchical synchronization and emergent complexity in the human connectome network

SUBJECT AREAS:

COMPLEX NETWORKS  
COMPUTATIONAL SCIENCE

Pablo Villegas, Paolo Moretti &amp; Miguel A. Muñoz

Departamento de Electromagnetismo y Física de la Materia e Instituto Carlos I de Física Teórica y Computacional. Universidad de Granada, E-18071 Granada, Spain.

Received  
17 April 2014Accepted  
18 June 2014Published  
8 August 2014Correspondence and  
requests for materials  
should be addressed to  
P.M. (moretti.paolo@  
gmail.com)

The spontaneous emergence of coherent behavior through synchronization plays a key role in neural function, and its anomalies often lie at the basis of pathologies. Here we employ a parsimonious (mesoscopic) approach to study analytically and computationally the synchronization (Kuramoto) dynamics on the actual human-brain connectome network. We elucidate the existence of a so-far-uncovered intermediate phase, placed between the standard synchronous and asynchronous phases, i.e. between order and disorder. This novel phase stems from the hierarchical modular organization of the connectome. Where one would expect a hierarchical synchronization process, we show that the interplay between structural bottlenecks and quenched intrinsic frequency heterogeneities at many different scales, gives rise to frustrated synchronization, metastability, and chimera-like states, resulting in a very rich and complex phenomenology. We uncover the origin of the dynamic freezing behind these features by using spectral graph theory and discuss how the emerging complex synchronization patterns relate to the need for the brain to access –in a robust though flexible way– a large variety of functional attractors and dynamical repertoires without *ad hoc* fine-tuning to a critical point.

Neuro-imaging techniques have allowed the reconstruction of structural human brain networks, composed of hundreds of neural regions and thousands of white-matter fiber interconnections. The resulting “human connectome” (HC)<sup>1,2</sup> turns out to be organized in moduli –characterized by a much larger intra than inter connectivity– structured in a hierarchical nested fashion across many scales<sup>3–10</sup>. On the other hand, “functional” connections between nodes in these networks have been empirically inferred from correlations in neural activity as detected in electroencephalogram and functional magnetic resonance time series. Unveiling how structural and functional networks influence and constrain each other is a task of utmost importance. A few pioneering works found that the hierarchical-modular organization of structural brain networks has profound implications for neural dynamics<sup>8,11–14</sup>. For example, neural activity propagates in hierarchical networks in a rather distinctive way, not observed on simpler networks<sup>15</sup>; beside the usual two phases –percolating and non-percolating– commonly encountered in models of activity propagation, an intermediate “Griffiths phase”<sup>16</sup> emerges on the hierarchical HC network<sup>15,17,18</sup>. Such a Griffiths phase stems from the existence of highly diverse relatively-isolated moduli or “rare regions” where neural activity remains mostly localized generating slow dynamics and very large responses to perturbations<sup>15–18</sup>.

Brain function requires coordinated or coherent neural activity at a wide range of scales, thus, neural synchronization is a major theme in neuroscience<sup>7,19,20</sup>. Synchronization plays a key role in vision<sup>21</sup>, memory<sup>22</sup>, neural communication<sup>23</sup>, and other cognitive functions<sup>24</sup>. An excess of synchrony results in pathologies such as epilepsy or Parkinsonian disease, while neurological deficit of synchronization has been related to autism and schizophrenia<sup>25</sup>.

Our aim here is to scrutinize the special features of synchronization dynamics<sup>26</sup> –as exemplified by the canonical Kuramoto model<sup>27–29</sup>– running on top of the best available human connectome mapping<sup>1,2,30</sup>. This consists of a network of 998 nodes, each of them representing a mesoscopic population of neurons –able to produce self-sustained oscillations<sup>31</sup>– whose mutual connections are encoded by a symmetric weighted connectivity matrix  $W^{1,2}$ . The validity of this admittedly simplistic Kuramoto model as a convenient tool to explore the generic features of complex brain dynamics at a large scales has been recently emphasized in the literature<sup>31–33</sup>. Here, we uncover the existence of a novel intermediate phase for synchronization dynamics –similar in spirit to the Griffiths phases discussed above– which stems from the hierarchical modular organization of the HC and which gives rise to very complex and rich synchronization dynamical patterns. We identify this novel phase as the

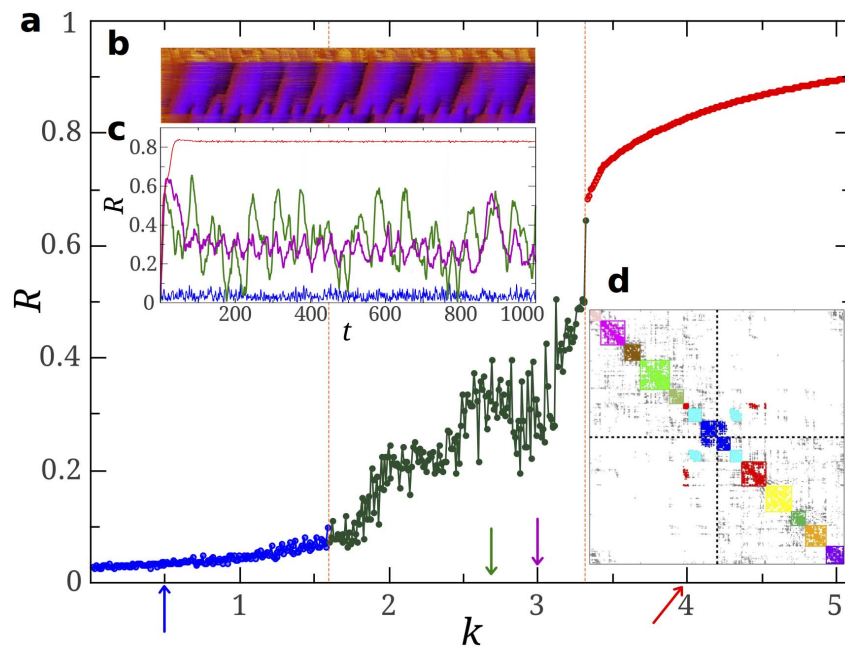


**Figure 1 | Global synchronization dynamics in the human connectome.** (a) Time average of the order parameter  $R(t)$ , for Kuramoto dynamics on the HC network for a specific and fixed set of frequencies extracted from a  $N(0, 1)$  Gaussian distribution. A broad intermediate regime separates the incoherent phase (low  $k$ ) from the synchronous one (high  $k$ ). In this regime, coherence increases with  $k$  in an intermittent fashion, and with strong dependence on the frequency realization. (b) Raster plot of individual phases (vertical axis) showing local rather than global synchrony and illustrating the coexistence of coherent and incoherent nodes ( $k = 2.7$ ) as time runs. (c)  $R(t)$  for 4 values of  $k$  (arrows in the main plot). (d) Adjacency matrix of the HC network with nodes ordered to emphasize its modular structure as highlighted by a community detection algorithm (main text), keeping the partition into the 2 hemispheres (dashed lines). Intra-modular connections (shown in color) are dense while inter-modular ones (grey) are limited to tiny subsets, acting as interfaces between moduli. Integration between hemispheres is mostly carried out by the 3 central moduli. This plot visually illustrates the hierarchical modular organization of the human connectome network.

optimal regime for the brain to harbor complex behavior, large dynamical repertoires, and optimal trade-offs between local segregation and global integration.

The Kuramoto dynamics on a generic network (see<sup>30</sup> for a nice and comprehensive review) is defined by:

$$\dot{\theta}_i(t) = \omega_i + k \sum_{j=1}^N W_{ij} \sin[\theta_j(t) - \theta_i(t)], \quad (1)$$

where  $\theta_i(t)$  is the phase at node  $i$  at time  $t$ . The intrinsic frequencies  $\omega_i$  – accounting for node heterogeneity – are extracted from some arbitrary distribution function  $g(\omega)$ ,  $W_{ij}$  are the elements of the  $N \times N$  connectivity matrix  $W$ , and  $k$  is the coupling strength. Time delays, noise, and phase frustration could also be straightforwardly implemented. The Kuramoto order parameter is defined as  $Z(t) = R(t)e^{i\psi(t)} = \langle e^{i\theta_i(t)} \rangle$ , where  $0 \leq R(t) \leq 1$  gauges the overall coherence and  $\psi(t)$  is the average global phase. In large populations of well-connected oscillators without frequency dispersion, perfect coherence ( $R = 1$ ) emerges for any coupling strength; on the other hand, frequency heterogeneity leads to a phase transition at some critical value of  $k$ , separating a coherent steady state from an incoherent one<sup>27–30</sup>. Analytical insight onto this phase transition can be obtained using the celebrated Ott-Antonsen (OA) ansatz, allowing for a projection of the high-dimensional dynamics into an evolution equation for  $Z(t)$  with remarkable accuracy in the large- $N$  limit<sup>34,35</sup>.

## Results

**Novel phase between order and disorder in the HC.** We have performed a computational study of the Kuramoto model running on top of the HC network (details are given in the Methods section). Our results reveal the existence of an intermediate regime placed between the coherent and the incoherent phase (see Fig. 1). This is characterized by broad quasi-periodic temporal oscillations of  $R(t)$

which wildly depend upon the realization of intrinsic frequencies<sup>36,37</sup>. Anomalously large sampling times would be required to extract good statistics for the actual mean values and variances. Collective oscillations of  $R(t)$  are a straightforward manifestation of partial synchronization and they are robust against changes in the frequency distribution (e.g. Gaussian, Lorentzian, uniform, etc.) whereas the location and width of the intermediate phase depend upon details. As this phenomenology is reminiscent of Griffiths phases –posed in between order and disorder and stemming from the existence of semi-isolated regions<sup>15–17</sup>– it is natural to investigate how the HC hierarchical modular structure affects synchronization dynamics.

Any network with perfectly isolated and independently synchronized moduli trivially exhibits oscillations of  $R(t)$ , with amplitude peaking at times when maximal mutual synchronization happens to be incidentally achieved. Such oscillations can become chaotic if a finite and relatively small number of different coherent moduli are coupled together<sup>38</sup>. Thus, in a connected network without delays or other additional ingredients, oscillations in the global coherence are the trademark of strong modular structure with weakly interconnected moduli.

Strong modular organization into distinct hierarchical levels is indeed present in the HC as revealed by standard community detection algorithms<sup>9,39</sup> and as already discussed in the literature (see e.g.<sup>15</sup> and references therein). For instance, we have found that the optimal partition into disjoint communities –i.e. the partition maximizing the modularity parameter<sup>40</sup>– corresponds to a division in 12 communities (see Fig. 1d) while, at a higher hierarchical level, a separation into just 2 moduli –the 2 cerebral hemispheres– is obtained<sup>2</sup> (Fig. 1d). Obviously these 2 coarser moduli include the 12 above as sub-moduli. Although more levels of hierarchical partitioning could be inferred (see e.g.<sup>10</sup> and refs. therein), for the sake of simplicity we focus on these two levels  $l$ ,  $l = 1$  and  $l = 2$  with 12 and 2 moduli, respectively.

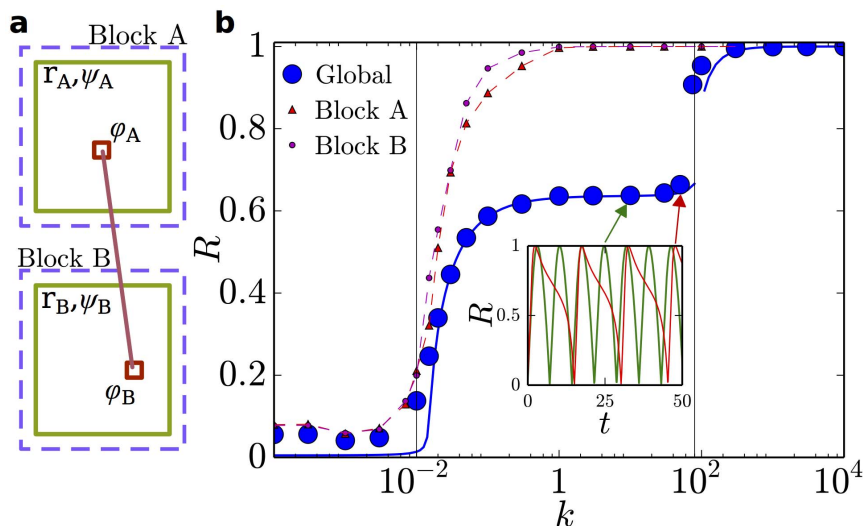


**Figure 2 | Two-block model.** (a) Sketch of the two-block model. (b) Global order parameter for the two-block model with  $M = 128$  and two interfacial nodes. Results of the numerical integration of the 258 Kuramoto equations (blue points) are in strikingly good agreement with the integration of Eqs.(2) (solid blue line). Local block-wise order parameters are shown for comparison (small symbols; dashed lines are guides to the eye). A first transition, where local order emerges, occurs at  $k \approx 0.02$ , while global coherence is reached at  $k \approx 90$ . In the intermediate region,  $R(t)$  oscillates (inset), revealing the lack of global coherence. Despite the simplicity of this toy model, these results constitute the essential building-block upon which further levels of complexity rely (see main text).

**A simplistic model for global oscillations.** To shed further light on the properties of synchronization on the HC, we consider a very simple network model –allowing for analytical understanding– which will constitute the elementary “building-block” for subsequent more complex analyses. This consists of a few blocks with very large internal connectivity and very sparse inter-connectivity. Each block is composed by a bulk of  $M \gg 1$  nodes that share no connection with the outside and a relatively small “interfacial” set that connects with nodes in other blocks. For instance, in the simplest realization, consisting of just two blocks connected by a single pair of nodes (Fig. 2), each block is endowed with local coherence  $r_{A,B}$ , average phase  $\psi_{A,B}$ , and average characteristic frequency  $\omega_{A,B}$ , while 1-node interfaces have perfect coherence  $r = 1$ , phase  $\varphi_{A,B}$ , and characteristic frequency  $\nu_{A,B}$ . In this case,  $N = 2M + 2$ , and the OA ansatz can be safely applied to each block (large  $M$ ) but not to single-node interfaces. In the particular case (convenient for analytical treatment) in which  $g(\omega)$  are zero-mean Lorentz distributions  $g(\omega) = \frac{1}{\pi} \frac{\delta}{(\omega - \Omega_0)^2 + \delta^2}$  with spreads  $\delta_{A,B}$ , the resulting set of OA equations can be easily shown to be:

$$\begin{aligned} \dot{\psi}_A &= \omega_A + k \frac{1+r_A^2}{2r_A} \sin(\varphi_A - \psi_A) \\ \dot{r}_A &= -\delta_A r_A + k \frac{1-r_A^2}{2} [Mr_A + \cos(\varphi_A - \psi_A)] \\ \dot{\varphi}_A &= \nu_A + k [Mr_A \sin(\psi_A - \varphi_A) + \sin(\varphi_B - \varphi_A)] \end{aligned} \quad (2)$$

(together with  $r = 1$  for each 1-node interface), and a symmetric set ( $A \leftrightarrow B$ ) for block B. The solution of Eq.(2) –displayed in Fig. 2– reveals a transition to local coherence within each block at a certain threshold value of  $k \approx 0.02$ . As soon as local order is attained,  $r_{A,B} \approx 1$  and  $\dot{\psi}_{A,B} \approx 0$ , from Eq.(2) the mutual synchronization process obeys

$$\dot{\varphi}_A \approx (\nu_A + M\omega_A) + k \sin(\varphi_B - \varphi_A) \quad (3)$$

and a symmetrical equation for  $\dot{\varphi}_B$ . For small  $k$ , the right-hand side is dominated by  $\nu_A + M\omega_A$ : whereas the average value  $\omega_A$  becomes arbitrarily small within blocks (assuming that  $M$  is large), the frequency  $\nu_A$  does not. Consequently, synchronization between the two blocks through the interfacial link is frustrated: each block remains inter-

nally synchronized but is unable to achieve coherence with the other over a broad interval of coupling strengths. This interval is delimited above by a second transition at  $k \sim \max\{M|\omega_{A,B}|, \nu_{A,B}\}$ , where  $k$  is large enough as to overcome frustration and generate global coherence. This picture is confirmed by numerical integration of the full system of  $N$  coupled Kuramoto equations as well as by its OA approximation (Eq.(2)), both in remarkably good agreement. Therefore, local and global coherences have their onsets at two well-separated transition points<sup>35</sup> and –similarly to the much more complex HC case–  $R$  oscillates in the intermediate regime (Fig. 2). Similar results hold for versions of the model with more than two moduli (e.g. 4; see below). The existence of two distinct (local and global) transitions had already been reported in a recent study of many blocks with much stronger inter-moduli connections than here<sup>35</sup> (even if, owing to this difference, no sign of an intermediate oscillatory phase was reported). In particular, the value of two-block models has already been explored in the past, for systems of identical oscillators with non-zero phase lags, in which each node is coupled equally to all the others in its community, and less strongly to those in the other<sup>41</sup>. In such systems, local coherence emerged for large enough values of the phase lag. Our two-block model shows that the presence of “structural bottlenecks” between moduli combined with heterogeneous frequencies at their contact nodes (interfaces) are essential ingredients to generate a broad region of global oscillations in  $R$ , even in the absence of phase lag. Still, it is obviously a too-simplistic model to account for all the rich phenomenology emerging on the HC, as we show now.

**Oscillations of local coherence in the HC.** Fig. 3 shows numerical results for the local order parameter  $r^{(l)}$  for some of the moduli at the 2 hierarchical levels,  $l = 1$  and  $l = 2$  in the HC network. It reveals that (Fig. 3a) local coherences exhibit oscillatory patterns in time (with characteristic frequencies typically between 0.01 and 0.1 Hz) and that (Fig. 3b) the transition to local coherence at progressively higher hierarchical level occurs at progressively larger values of  $k$ ; i.e. coherence emerges out of a hierarchical bottom-up process as illustrated above for the two-block model (see<sup>35,42</sup>). Observe, however, that local oscillations were not present in the two-block model. This suggests that the 12 moduli in the HC are on their turn composed of finer sub-moduli and that structural frustration, as

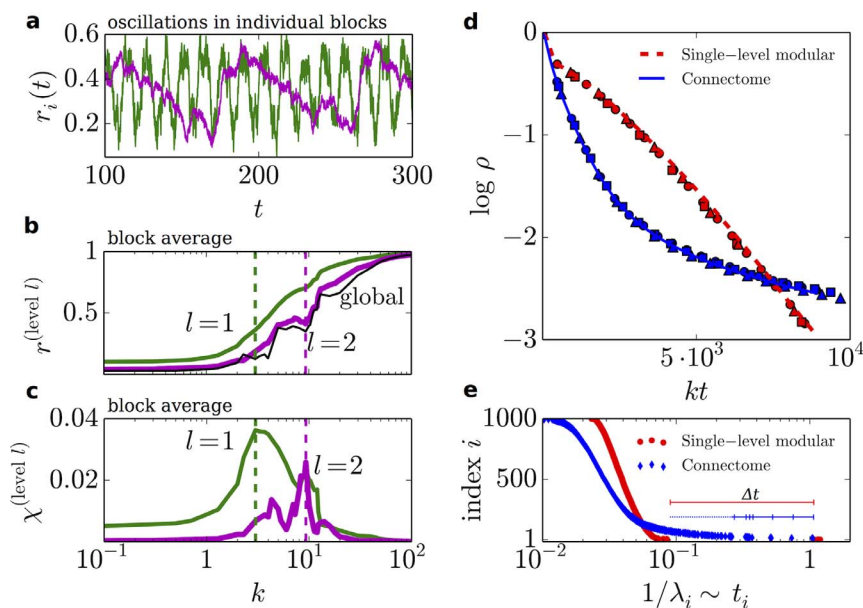


**Figure 3 | Local synchronization in the human connectome.** (a) Oscillations of the local order parameters (“chimera-like states”) in one particular modulus in the partitions of the HC into 12 (green,  $l = 1$ , and  $k = 3$ ) and 2 (magenta,  $l = 2$ , and  $k = 10$ ) moduli, respectively. The characteristic frequency of these oscillations is typically between 0.01 and 0.1 Hz (a range which coincides with slow modes detected in brain activity; see e.g.<sup>32</sup>). (b) Average of the local order parameter over all moduli and (c) chimera index for moduli at levels as in a), as a function of  $k$ . Global order (thin black line in b)) emerges only after local order is attained at lower levels. (d) Average decay of activity  $\rho$  for identical frequencies  $\omega = 0$  in the HC network and comparison with a single-level modular network (made up of 4 similar random moduli at a single hierarchical level) of the same size and average connectivity as the HC network. Symbols stand for different values of  $k$ . (e) Characteristic decay times corresponding to the inverse of the first 1000 non-trivial eigenvalues of the Laplacian matrix (x axis) as a function of their respective ordered indices (y axis), for networks as in (d). The stretched exponential behavior in (d) is the result of the convolution of slow time scales associated with small eigenvalues in (e).

introduced above, affects all hierarchical levels. The average variance of local coherences (called chimera index,  $\chi$ )<sup>44</sup> exhibits a marked peak –reflecting maximal configurational variability– at the transition point for the corresponding level (Fig. 3b–c and Methods section). Similar intra-modular oscillatory patterns –dubbed *chimera states*– have been recently found<sup>41,43–45</sup> in Kuramoto models in which explicit phase lags induce a different kind of frustration, hindering global synchronization. Strictly speaking, chimeras are defined in systems of identical oscillators. In such a case, a non-zero phase lag term is essential for partial synchronization to occur. Realistic models of the brain, however, require oscillators to be heterogeneous. States of partial synchronization in empirical brain networks with frequency heterogeneity have been found for Kuramoto models with explicit time delays<sup>31</sup>. In contrast, the chimera-like states put forward here have a purely structural origin, as they arise from the network topology. It was noted in the past that synchronization in a synthetic network with hubs could be limited to those hubs by tuning clustering properties, and global order could be attained in a monotonous step-like fashion upon increasing  $k$ <sup>46</sup>. Fig. 3b instead reveals that the ordering process in the hierarchical modular HC may be non-monotonous: coherence does not systematically grow with  $k$ . Indeed, the emergence of local order in some community may hinder or reduce coherence in others, inducing local “desynchronization” and reflecting the metastable nature of the explored states.

**Anomalous dynamics on the HC.** Fixing all intrinsic frequencies to be identical allows us to focus specifically on structural effects. Thus, we consider, without loss of generality, the simple case  $\omega_i = 0$ , and define the “activity”  $\rho = 1 - \langle R \rangle$ . In this case, perfect asymptotic coherence should emerge for all values of  $k$  but, as illustrated in Fig. 3d, the convergence towards  $\rho = 0$  turns out to be extremely slow (much slower than exponential). This effect can be analytically investigated assuming that, for large enough times, all phase diffe-

rences are relatively small. Then, up to first order,  $\dot{\theta}_i = -k \sum_j L_{ij} \theta_j$  where  $L_{ij} = \delta_{ij} \sum_l W_{jl} - W_{ij}$  are the elements of the Laplacian matrix<sup>47,48</sup>. Solving the linear problem,  $\theta_i(t) = \sum_{l,j} e^{-k\lambda_l t} v_l^i v_j^l \theta_j(0)$ , where  $\lambda_l$  denotes the  $l$ -th Laplacian eigenvalue ( $0 = \lambda_1 < \lambda_2 < \dots < \lambda_N$ ) and  $v_l^i$  the  $i$ -th component of the corresponding eigenvector. Given that the averaged order parameter can be written as  $Z(t) \approx \sum_j \left( 1 + i\theta_j - \frac{1}{2}\theta_j^2 \right) / N$ , averaging over initial conditions, and considering that (as the Laplacian has zero row-sums<sup>48</sup>)  $\lambda_1 = 0$ , we obtain

$$\rho(t) = \frac{\sigma^2}{2} \sum_{l=2}^N e^{-2k\lambda_l t}, \quad (4)$$

where  $\sigma$  is the standard deviation of the initial phases. This expression holds for any connected network. As usual, the larger the spectral gap  $\lambda_2$ , the more “entangled”<sup>48</sup> the network and thus the more difficult to divide it into well separated moduli ( $\lambda_2 = 0$  only for disconnected networks)<sup>47,48</sup>. For large spectral gaps all timescales are fast, and the last expression can be approximated by its leading contribution, ensuing exponential relaxation to  $\rho = 0$ , as in fact observed in well-connected network architectures (Erdős-Rényi, scale free, etc.<sup>40</sup>). This is not the case for the HC matrix, for which a tail of small non-degenerate eigenvalues is encountered (see Fig. 3e and<sup>15</sup>). Each eigenvalue  $\lambda_i$  in the tail corresponds to a natural division of moduli into submoduli<sup>48</sup>, and the broad tail reflects the heterogeneity in the resulting modular sizes. As a consequence, each of these eigenvalues –with its associated large timescale,  $t_i = 1/\lambda_i$ – contributes to the sum above, giving rise to a convolution of relaxation processes, entailing anomalously-slow dynamics, which could not be explained by a single-level modular network (see Fig. 3d–e): slow dynamics necessarily stems from the existence of a





hierarchy of moduli and structural bottlenecks. As explained in Methods, in the case of the HC the convolution of different times scales gives rise to stretched-exponential decay, which perfectly fits with numerical results in Fig. 3. It was noted in the past that strongly modular networks exhibit isolated eigenvalues in the lower edge of the laplacian spectrum. Synchronization would develop in a step-wise process in time, where each transient would be given by each isolated eigenvalue<sup>42</sup>. In our case, the depth of the hierarchical organization and the strength of topological disorder produce instead a quasi-continuous tail of eigenvalues, and the step-wise process is replaced by an anomalous stretched-exponential behavior.

#### A more refined model: hierarchical modular synthetic networks.

To shed additional light on the previous findings for the HC –i.e. the emergence of chimera-like states and anomalously slow dynamics– we suggest to go beyond the single-level modular network model and study hierarchical modular networks (HMN) in which moduli exists within moduli in a nested way at various scales<sup>3–6,8,9</sup>. HMN are assembled in a bottom-up fashion: local fully-connected moduli (e.g. of 16 nodes) are used as building blocks. They are recursively grouped by establishing additional inter-moduli links in a level-dependent way as sketched in Fig. 4(top)<sup>15,49</sup>.

Our computational analyses of the Kuramoto dynamics on HMN substrates (see Fig. 4) reveal: (i) a sequence of synchronization transitions for progressively higher hierarchical levels at increasing values of  $k$ , (ii) chimera-like states at every hierarchical level, resulting in a hierarchy of metastable states with maximal variability at the corresponding transition points, (iii) extremely slow relaxation toward the coherent state when all internal frequencies are identical. Furthermore, anomalies in the Laplacian spectrum analogous to those of the HC network are observed for HMN matrices; in particular, the lower edge of the HMN Laplacian spectrum has been recently

shown to exhibit a continuous exponential Lifshitz tail  $p(\lambda) \sim e^{-1/\lambda^\alpha}$  for  $N \rightarrow \infty$ , with  $\alpha \approx 1^{15}$ . Taking the continuum limit of Eq.(4), we find  $\rho(t) \approx \frac{\sigma^2}{2} \int d\lambda p(\lambda) e^{-2k\lambda t}$ , which can be evaluated with the saddle-point method (see Methods), leading to

$$\rho(t) \sim e^{-\sqrt{8kt}}, \quad (5)$$

i.e. anomalous stretched-exponential asymptotic behavior, in excellent agreement with computational results (see Fig. 4d). Therefore, hierarchical modular networks constitute a parsimonious and adequate model for reproducing all the complex synchronization phenomenology of the HC.

A crucial role in the emergence of such behavior is played by disorder. One would be tempted to believe that all networks characterized by a finite spectral dimension could potentially give rise to this phenomenology. This is obviously not the case for a regular lattice, where the spectral gap is always well defined. A fractal lattice or an ordered tree, on the other hand, could exhibit a hierarchy of discrete low eigenvalues, whose multiplicities reflect system symmetries. The introduction of disorder, as in HMNs, is then necessary in order to transform such hierarchy of discrete levels into a continuous Lifshitz tail, leading eventually to the behavior predicted by Eq. (5).

#### Discussion

Simple models of synchronization dynamics exhibit an unexpectedly rich phenomenology when operating on top of empirical human brain networks. This complexity includes oscillatory behavior of the order parameter suggesting the existence of relatively isolated structural communities or moduli, that –as a matter of fact– can be identified by using standard community detection algorithms. Even more remarkably, oscillations in the level of internal coherence

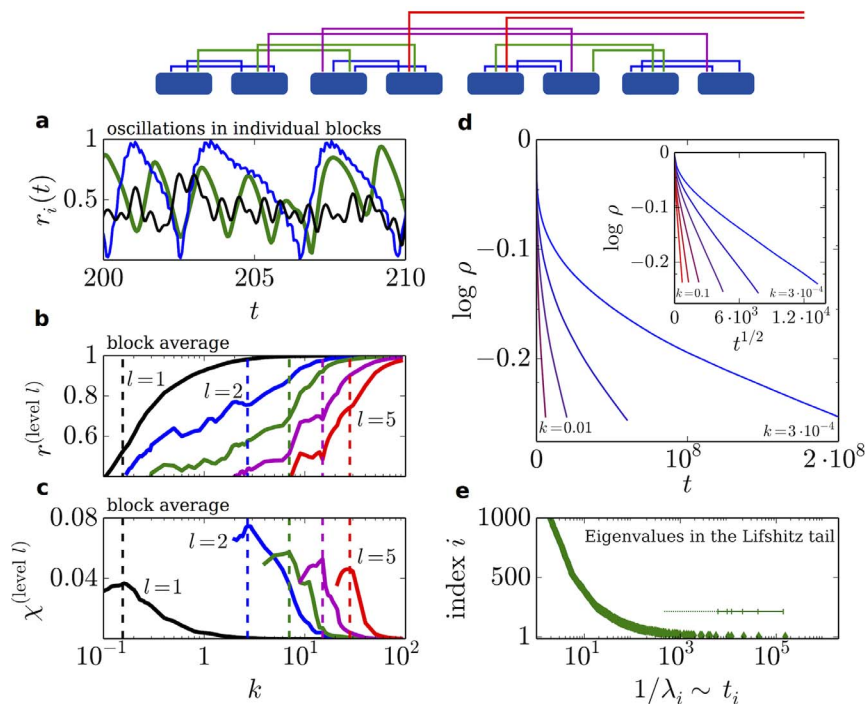


**Figure 4 | Synchronization in hierarchical modular networks.** Top panel: sketch of the HMN model. At hierarchical level 1,  $2^s$  basal fully connected blocks of size  $M$  are linked pairwise into super-blocks by establishing a fixed number  $\alpha$  of random unweighted links between the elements of each ( $\alpha = 2$  in the Fig.). Newly formed blocks are then linked iteratively with the same  $\alpha$  up to level  $s$ , until the network becomes connected. (a), (b), (c) as in Fig. 3, but for a HMN with  $N = 512$ ,  $s = 5$ , and  $\alpha = 4$ . Hierarchical levels are  $i = 1 \rightarrow 5$  in black, blue, green, magenta and red respectively (not all shown in a) for clarity). (d) Time relaxation of activity  $\rho$  for homogeneous characteristic frequencies  $\omega = 0$ , for logarithmically equally spaced values of  $k$ . Averages over  $10^6$  realizations of HMNs with  $N = 4096$  and  $s = 11$ . Inset: as in the main plot (d), but representing as a function of  $t^{1/2}$  and confirming the predicted stretched exponential behavior. (e) Inverse tail-eigenvalues (as in Fig. 3) for a HMN as in e).



are also present within these moduli, suggesting the existence of a whole hierarchy of nested levels of organization, as also found in the recent literature relying on a variety of approaches<sup>3–10</sup>. Aimed at unveiling this complex behavior we have introduced a family of hierarchical modular networks and studied them in order to assess what structural properties are required in order to reproduce the complex synchronization patterns observed in brain networks.

In the absence of frequency dispersion, perfect coherence is achieved in synthetic hierarchical networks by following a bottom-up ordering dynamics in which progressively larger communities – with inherently different timescales – become coherent (see<sup>42</sup>). However, this hierarchically nested synchronization process is constrained and altered by structural bottlenecks – as carefully described here for the simpler two-block toy model – at all hierarchical levels. This structural complexity brings about anomalously-slow dynamics at very large timescales. Observe that the HC, in spite of being a coarse-grained mapping of a brain network, already shows strong signals of this ideal hierarchical architecture as reflected in its anomalously slow synchronization dynamics as well as in the presence of non-degenerate eigenvalues in the lower edge of its Laplacian spectrum, acting as a fingerprint of structural heterogeneity and complexity. We stress that such a complex phenomenology would be impossible to obtain in networks with stronger connectivity patterns (e.g. with the small world property) such as scale free-networks or high-degree random graphs. Even the generic presence of simple communities may not be sufficient to grant the emergence of frustration: the uniqueness of the human connectome, and of hierarchical modular networks in general, resides in the strong separation into distinct levels, which the synchronization dynamics is able to resolve only at well-separated values of the coupling  $k$ .

On the other hand, in the presence of intrinsic frequency heterogeneity, the described slow ordering process is further frustrated. Actually, for small values of the coupling constant  $k$  the system remains trapped into metastable and chimera-like states with traits of local coherence at different hierarchical levels. In this case, inter-moduli frequency barriers need to be overcome before weakly connected moduli achieve mutual coherence. This is clearly exemplified by the separation between distinct peaks in the chimera index  $\chi^{(l)}$  in Figs. 3–4, each one signaling the onset of an independent synchronization process at a given level (see Methods). The result is a complex synchronization landscape, which is especially rich and diverse in the intermediate regime put forward here.

Including other realistic ingredients such as explicit phase frustration<sup>44</sup> or time delays<sup>31,45</sup> to our simplistic approach should only add complexity to the structural frustration effect reported here. It is also expected that more refined models – including neuro-realistic ingredients leading to collective oscillations – would generate similar results, but this remains to be explored in future works.

Addition of noise to the Kuramoto dynamics would allow the system to escape from metastable states. Stochasticity can overcome the “potential barriers” between mutually incoherent moduli as well as re-introduce de-synchronization effects. These combined effects can make the system able to explore the nested hierarchy of attractors, allowing one to shed some light into the complex synchronization patterns in real brain networks. Actually, spontaneous dynamical fluctuations have been measured in the resting state of human brains<sup>50</sup>; these are correlated across diverse segregated moduli and characterized by very slow fluctuations, of typical frequency  $< 0.1$  Hz, in close agreement with those found here (Fig. 3). Accordingly, it has been suggested that the brain is routinely exploring different states or attractors<sup>51</sup> and that – in order to enhance spontaneous switching between attractors – brain networks should operate close to a critical point, allowing for large intrinsic fluctuations which on their turn entail attractor “surfing” and give access to highly varied functional configurations<sup>51–55</sup> and, in particular, to maximal variability of phase synchrony<sup>56</sup>.

The existence of multiple attractors and noise-induced surfing is largely facilitated in the broad intermediate regime first elucidated here, implying that a precise fine tuning to a critical point might not be required to guarantee functional advantages usually associated with criticality<sup>52,57,58</sup>: the role usually played by a critical point is assumed by a broad intermediate region in hierarchically architected complex systems<sup>15</sup>. Finally, let us remark that our results might also be of relevance for other hierarchically organized systems such as gene regulatory networks<sup>59</sup> for which coherent activations play a pivotal role<sup>60</sup>.

## Methods

**Numerical simulation of the Kuramoto model.** The Kuramoto model is simulated by numerically integrating Eq. (1). Computations are carried out using both a 4th order Runge-Kutta method of fixed step size  $h = 10^{-3}$  and an 8th order Dormand-Prince method with adaptive step size. Both methods lead to compatible results within precision limits. The robustness of the observation of a novel intermediate phase – between incoherent and coherent ones – is assessed by choosing different functional forms for the frequency distribution  $g(\omega)$  (Lorentzian, Gaussian, uniform), and by implementing variations of Eq. 1 in which the matrix  $W$  is weight-normalized<sup>30</sup> for simulations of the HC and degree-normalized for simulations in HMNs. No qualitative change in the phenomenology is observed.

**Chimera index  $\chi^{(l)}$  and hierarchical synchronization.** In the main text, the chimera index  $\chi^{(l)}$  is introduced as a measure of partial synchronization at the community level  $l$ . At any hierarchical level  $l$ , a hierarchical network can be divided into a set of communities. Following<sup>44</sup>,  $\chi^{(l)}$  is defined as follows: (i) in the steady (oscillatory) state, and for each time  $t$ , local order parameters  $r_i^{(l)}(t)$  for each community  $i$  are calculated and their variance across communities  $\sigma_{\text{ch}}^{(l)}(t)$  is stored; (ii) the chimera index is computed as the time average  $\chi^{(l)} = \left\langle \sigma_{\text{ch}}^{(l)}(t) \right\rangle_t$ . Having  $\chi^{(l)} > 0$  at a given hierarchical level  $l$  implies that local order is only partial as  $r_i^{(l)}$  fluctuates, giving rise to a chimera-like state. On the other hand,  $\chi^{(l)} = 0$  means that each local order parameter at that level is  $r_i^{(l)} \approx 1$ , and local order has been attained. Figs. 3b–c and 4b–c show that at each  $l$  (each color) a peak in the corresponding  $\chi^{(l)}$  marks the onset of the local synchronization processes: as soon as the peak vanishes upon increasing  $k$ , local order at that level is attained. The sequence of separated peaks in  $\chi^{(l)}$  for increasing values of  $l$  is the direct evidence of a hierarchical synchronization process.

**Lifshitz tail and stretched-exponential asymptotic behavior.** In sparse HMNs, the lower end of the Laplacian spectrum is characterized by an exponential tail in the density of states  $p(\lambda) \sim e^{-1/\lambda^a}$ , known as Lifshitz tail<sup>15</sup>. In graphs, Lifshitz tails signal the existence of non-trivial heterogeneous localized states governing the asymptotic synchronization dynamics at very large times  $t$ . In the main text we have shown that in the absence of frequency heterogeneity, the  $t \rightarrow \infty$  behavior of the activity is given by  $\rho(t) \approx \frac{\sigma^2}{2} \int d\lambda p(\lambda) e^{-2k\lambda t}$ . This expression can be evaluated by applying the saddle point method, yielding

$$\rho(t) \approx \frac{\sigma^2}{2} \exp \left[ - (1+a) a^{-\frac{a}{1+a}} (2kt)^{\frac{a}{1+a}} \right]. \quad (6)$$

Substituting  $a \approx 1$ , as empirically found in HMNs<sup>15</sup>, leads to Eq. (5), whose square root behavior is confirmed by simulations in Fig. 4d.

- Hagmann, P. *et al.* Mapping the structural core of human cerebral cortex. *PLoS Biol.* **6**, e159 (2008).
- Honey, C. J. *et al.* Predicting human resting-state functional connectivity from structural connectivity. *Proc. Natl. Acad. Sci. USA* **106**, 2035–2040 (2009).
- Bullmore, E. & Sporns, O. Complex brain networks: graph theoretical analysis of structural and functional systems. *Nat. Rev. Neurosci.* **10**, 186–198 (2009).
- Sporns, O. *Networks of the Brain*. (MIT Press, Cambridge, 2010).
- Kaiser, M. A tutorial in connectome analysis: topological and spatial features of brain networks. *NeuroImage* **57**, 892–907 (2011).
- Meunier, D., Lambiotte, R. & Bullmore, E. Modular and hierarchically modular organization of brain networks. *Front. Neurosci.* **4**, 200 (2010).
- Buzsáki, G. *Rhythms of the Brain*. (Oxford University Press, New York, 2006).
- Zhou, C., Zemanová, L., Zamora, G., Hilgetag, C. C. & Kurths, J. Hierarchical organization unveiled by functional connectivity in complex brain networks. *Phys. Rev. Lett.* **97**, 238103 (2006).
- Ivković, M., Amy, K. & Ashish, R. Statistics of weighted brain networks reveal hierarchical organization and gaussian degree distribution. *PLoS ONE* **7**, e35029 (2012).
- Betz, R. F. *et al.* Multi-scale community organization of the human structural connectome and its relationship with resting-state functional connectivity. *Network Science* **1**, 353–373 (2013).



11. Zhou, C., Zemanová, L., Zamora-López, G., Hilgetag, C. C. & Kurths, J. Structure–function relationship in complex brain networks expressed by hierarchical synchronization. *New J. Phys.* **9**, 178 (2007).
12. Kaiser, M., Görner, M. & Hilgetag, C. C. Criticality of spreading dynamics in hierarchical cluster networks without inhibition. *New J. Phys.* **9**, 110 (2007).
13. Kaiser, M. & Hilgetag, C. C. Optimal hierarchical modular topologies for producing limited sustained activation of neural networks. *Front. Neuroinform.* **4**, 8 (2010).
14. Rubinov, M., Sporns, O., Thivierge, J. P. & Breakspear, M. Neurobiologically realistic determinants of self-organized criticality in networks of spiking neurons. *PLoS Comput. Biol.* **7**, e1002038 (2011).
15. Moretti, P. & Muñoz, M. A. Griffiths phases and the stretching of criticality in brain networks. *Nat. Commun.* **4**, 2521 (2013).
16. Vojta, T. Rare region effects at classical, quantum and nonequilibrium phase transitions. *J. Phys. A* **39**, R143–R205 (2006).
17. Muñoz, M. A., Juhász, R., Castellano, C. & Odor, G. Griffiths Phases on Complex Networks. *Phys. Rev. Lett.* **105**, 128701 (2010).
18. Juhász, R., Odor, G., Castellano, C. & Muñoz, M. A. Rare-region effects in the contact process on networks. *Phys. Rev. E* **85**, 066125 (2012).
19. Bennett, M. V. & Zukin, R. Electrical coupling and neuronal synchronization in the mammalian brain. *Neuron* **41**, 495–511 (2004).
20. Breakspear, M. & Stam, C. J. Dynamics of a neural system with a multiscale architecture. *Phil. Trans. R. Soc. Lond. B* **360**, 1051–1074 (2005).
21. Sompolinsky, H., Crisanti, A. & Sommers, H. J. Chaos in random neural networks. *Phys. Rev. Lett.* **61**, 259–262 (1988).
22. Klimesch, W. Memory processes, brain oscillations and EEG synchronization. *Int. J. Psychophysiol.* **24**, 61–100 (1996).
23. Buehlmann, A. & Deco, G. Optimal information transfer in the cortex through synchronization. *PLoS Comput. Biol.* **6**, e1000934 (2010).
24. Steinmetz, P. N. *et al.* Attention modulates synchronized neuronal firing in primate somatosensory cortex. *Nature* **404**, 187–190 (2000).
25. Kandel, E. R., Schwartz, J. H. & Jessell, T. M. *Principles of Neural Science*. (McGraw-Hill, New York, 2000).
26. Rosenblum, M. G., Pikovsky, A. & Kurths, J. *Synchronization – A universal concept in nonlinear sciences*. (Cambridge University Press, Cambridge, 2001).
27. Kuramoto, Y. Self-entrainment of a population of coupled nonlinear oscillators. *Lect. Notes Phys.* **39**, 420–422 (1975).
28. Strogatz, S. H. From Kuramoto to Crawford: exploring the onset of synchronization in populations of coupled oscillators. *Physica D* **143**, 1–20 (2000).
29. Acebrón, J. A., Bonilla, L. L., Pérez Vicente, C. J., Ritort, F. & Spigler, R. The Kuramoto model: a simple paradigm for synchronization phenomena. *Rev. Mod. Phys.* **77**, 137–185 (2005).
30. Arenas, A., Díaz-Guilera, A., Kurths, J., Moreno, Y. & Zhou, C. Synchronization in complex networks. *Phys. Rep.* **469**, 93–153 (2008).
31. Cabral, J., Hugues, E., Sporns, O. & Deco, G. Role of local network oscillations in resting-state functional connectivity. *NeuroImage* **57**, 130–139 (2011).
32. Breakspear, M., Heitmann, S. & Daffertshofer, A. Generative models of cortical oscillations: neurobiological implications of the Kuramoto model. *Front. Hum. Neurosci.* **4**, 190 (2010).
33. Gómez-Gardeñes, J., Zamora-López, G., Moreno, Y. & Arenas, A. From modular to centralized organization of synchronization in functional areas of the cat cerebral cortex. *PLoS One* **5**, e12313 (2010).
34. Ott, E. & Antonsen, T. M. Low dimensional behavior of large systems of globally coupled oscillators. *Chaos* **18**, 037113 (2008).
35. Skardal, P. S. & Restrepo, J. G. Hierarchical synchrony of phase oscillators in modular networks. *Phys. Rev. E* **85**, 016208 (2012).
36. Arenas, A. & Pérez-Vicente, C. J. Exact long-time behavior of a network of phase oscillators under random fields. *Phys. Rev. E* **50**, 949–956 (1994).
37. Acebrón, J. A. & Bonilla, L. L. Asymptotic description of transients and synchronized states of globally coupled oscillators. *Physica D* **114**, 296–314 (1998).
38. Popovych, O. V., Maistrenko, Y. L. & Tass, P. A. Phase chaos in coupled oscillators. *Phys. Rev. E* **71**, 065201 (2005).
39. Duch, J. & Arenas, A. Community detection in complex networks using extremal optimization. *Phys. Rev. E* **72**, 027104 (2005).
40. Newman, M. The Structure and Function of Complex Networks. *SIAM Rev.* **45**, 167–256 (2003).
41. Abrams, D. M. & Strogatz, S. H. Chimera States for Coupled Oscillators. *Phys. Rev. Lett.* **93**, 174102 (2004).
42. Arenas, A., Díaz-Guilera, A. & Pérez-Vicente, C. J. Synchronization reveals topological scales in complex networks. *Phys. Rev. Lett.* **96**, 114102 (2006).
43. Abrams, D. M., Mirollo, R., Strogatz, S. H. & Wiley, D. A. Solvable model for chimera states of coupled oscillators. *Phys. Rev. Lett.* **101**, 084103 (2008).
44. Shanahan, M. Metastable chimera states in community-structured oscillator networks. *Chaos* **20**, 013108 (2010).
45. Wildie, M. & Shanahan, M. Metastability and chimera states in modular delay and pulse-coupled oscillator networks. *Chaos* **22**, 043131 (2012).
46. McGraw, P. N. & Menzinger, M. Clustering and the synchronization of oscillator networks. *Phys. Rev. E* **72**, 015101(R) (2005).
47. Chung, F. R. K. *Spectral graph theory*. (Reg. Conf. Series. in Maths, AMS, Providence, 1997).
48. Donetti, L., Neri, R. & Muñoz, M. A. Optimal network topologies: expanders, cages, Ramanujan graphs, entangled networks and all that. *J. Stat. Mech.* P08007 (2006).
49. Wang, S.-J., Hilgetag, C. C. & Zhou, C. Sustained activity in hierarchical modular neural networks: SOC and oscillations. *Front. Comput. Neurosci.* **5**, 30 (2011).
50. Biswal, B., Zerrin Yetkin, F., Haughton, V. & Hyde, J. Functional connectivity in the motor cortex of resting human brain using echo-planar MRI. *Magnet. Reson. Med.* **34**, 537–541 (1995).
51. Deco, G. & Jirsa, V. K. Ongoing cortical activity at rest: criticality, multistability, and ghost attractors. *J. Neurosci.* **32**, 3366–3375 (2012).
52. Chialvo, D. R. Emergent complex neural dynamics. *Nat. Phys.* **6**, 744–750 (2010).
53. Shew, W. L., Yang, H., Petermann, T., Roy, R. & Plenz, D. Neuronal avalanches imply maximum dynamic range in cortical networks at criticality. *J. Neurosci.* **29**, 15595–15600 (2009).
54. Haimovici, A., Tagliazucchi, E., Balenzuela, P. & Chialvo, D. R. Brain organization into resting state networks emerges at criticality on a model of the human connectome. *Phys. Rev. Lett.* **110**, 178101 (2013).
55. Shriki, O. *et al.* Neuronal avalanches in the resting MEG of the human brain. *J. Neurosci.* **33**, 7079–7090 (2013).
56. Yang, H., Shew, W. L., Roy, R. & Plenz, D. Maximal variability of phase synchrony in cortical networks with neuronal avalanches. *J. Neurosci.* **32**, 1061–1072 (2012).
57. Beggs, J. M. The criticality hypothesis: how local cortical networks might optimize information processing. *Phil. Trans. R. Soc. A* **366**, 329–343 (2008).
58. Shew, W. L. & Plenz, D. The functional benefits of criticality in the cortex. *Neuroscientist* **19**, 88–100 (2013).
59. Treviño III, S., Sun, Y., Cooper, T. F. & Bassler, K. Robust detection of hierarchical communities from *Escherichia coli* gene expression data. *PLoS Comput. Biol.* **8**, e1002391 (2012).
60. Nykter, M. *et al.* Gene expression dynamics in the macrophage exhibit criticality. *Proc. Natl. Acad. Sci. USA* **105**, 1897–1900 (2008).

## Acknowledgments

We acknowledge financial support from J. de Andalucía, grant P09-FQM-4682 and we thank O. Sporns for providing us access to the human connectome data.

## Author contributions

P.M. and M.A.M. conceived the project, P.V. and P.M. performed the numerical simulations, carried out the analytical calculations and prepared the figures. P.M. and M.A.M. wrote the main manuscript text. All authors reviewed the manuscript.

## Additional information

**Competing financial interests:** The authors declare no competing financial interests.

**How to cite this article:** Villegas, P., Moretti, P. & Muñoz, M.A. Frustrated hierarchical synchronization and emergent complexity in the human connectome network. *Sci. Rep.* **4**, 5990; DOI:10.1038/srep05990 (2014).



This work is licensed under a Creative Commons Attribution-NonCommercial-ShareAlike 4.0 International License. The images or other third party material in this article are included in the article's Creative Commons license, unless indicated otherwise in the credit line; if the material is not included under the Creative Commons license, users will need to obtain permission from the license holder in order to reproduce the material. To view a copy of this license, visit <http://creativecommons.org/licenses/by-nc-sa/4.0/>